

## Spectroscopic Demonstration of a Large Antisymmetric Exchange Contribution to the Spin-Frustrated Ground State of a $D_3$ Symmetric Hydroxy-Bridged Trinuclear Cu(II) Complex: Ground-to-Excited State Superexchange Pathways

Jungjoo Yoon, Liviu M. Mirica, T. Daniel P. Stack,\* and Edward I. Solomon\*

Contribution from the Department of Chemistry, Stanford University, Stanford, California 94305

Received June 18, 2004; E-mail: edward.solomon@stanford.edu; stack@stanford.edu

**Abstract:** The magnetic and electronic properties of a spin-frustrated ground state of an antiferromagnetically coupled 3-fold symmetric trinuclear copper complex (TrisOH) is investigated using a combination of variable-temperature variable-field magnetic circular dichroism (VTVH MCD) and powder/single-crystal EPR. Direct evidence for a low-lying excited  $S = 1/2$  state from the zero-field split ground  $^2E$  state is provided by the nonlinear dependence of the MCD intensity on  $1/T$  and the nesting of the VTVH MCD isotherms. A consistent zero-field splitting ( $\Delta$ ) value of  $\sim 65 \text{ cm}^{-1}$  is obtained from both approaches. In addition, the strong angular dependence of the single-crystal EPR spectrum, with effective  $g$ -values from 2.32 down to an unprecedented 1.2, requires in-state spin-orbit coupling of the  $^2E$  state via antisymmetric exchange. The observable EPR intensities also require lowering of the symmetry of the trimer structure, likely reflecting a magnetic Jahn-Teller effect. Thus, the  $\Delta$  of the ground  $^2E$  state is shown to be governed by the competing effects of antisymmetric exchange ( $G = 36.0 \pm 0.8 \text{ cm}^{-1}$ ) and symmetry lowering ( $\delta = 17.5 \pm 5.0 \text{ cm}^{-1}$ ).  $G$  and  $\delta$  have opposite effects on the spin distribution over the three metal sites where the former tends to delocalize and the latter tends to localize the spin of the  $S_{\text{tot}} = 1/2$  ground state on one metal center. The combined effects lead to partial delocalization, reflected by the observed EPR parallel hyperfine splitting of  $74 \times 10^{-4} \text{ cm}^{-1}$ . The origin of the large  $G$  value derives from the efficient superexchange pathway available between the ground  $d_{x^2-y^2}$  and excited  $d_{xy}$  orbitals of adjacent Cu sites, via strong  $\sigma$ -type bonds with the in-plane p-orbitals of the bridging hydroxy ligands. This study provides significant insight into the orbital origin of the spin Hamiltonian parameters of a spin-frustrated ground state of a trigonal copper cluster.

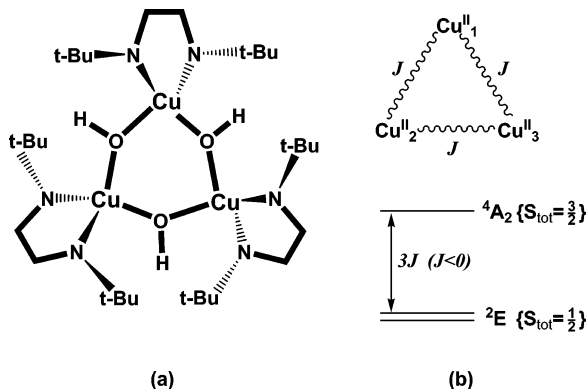
### Introduction

Simple polynuclear paramagnetic metal clusters have become indispensable in the study of systems in biology<sup>1,2</sup> and magnetic materials,<sup>3</sup> as they allow one to develop a detailed understanding of the electronic and magnetic properties and, thus, the fundamental bonding description of more complex analogues. Of these, copper trimers with trigonal symmetry<sup>4–13</sup> have attracted significant interest, as these complexes resemble the active sites of the multicopper oxidases<sup>14</sup> (laccase, ascorbate oxidase, ceruloplasmin, CueO, Fet3p, etc.) which reduce  $\text{O}_2$  to  $\text{H}_2\text{O}$ . The structures of the active site are known through both spectroscopy<sup>15</sup> and X-ray crystallography.<sup>16</sup> In particular, a recent spectroscopic study<sup>15c</sup> has shown that the “native intermediate” in  $\text{O}_2$  reduction has a fully oxidized antiferromagnetically coupled trinuclear  $\text{Cu}^{\text{II}}$  cluster, in which all copper atoms are bridged by the oxygen atoms resulting from the complete four-electron reduction of  $\text{O}_2$ .

The basic description of an exchange coupled trinuclear copper complex is given by the isotropic exchange Hamiltonian of the form  $H = -2J \sum_{i,j} S_i S_j$ , i.e., the Heisenberg, Dirac, Van Vleck (HDVV) model.<sup>17,18</sup> Each of the three spins can interact with its adjacent spins as shown in Scheme 1b. Two  $\text{Cu}^{\text{II}}$  atoms with  $S = 1/2$  couple to form intermediate spins  $S' = 1$  and 0; these then couple to the third  $\text{Cu}^{\text{II}}$  atom with  $S = 1/2$  to give  $S_{\text{tot}}$

- (1) See the thematic (Biomimetic Inorganic Chemistry) issue of *Chem. Rev.* **2004**, *104* (2), 347–1200.
- (2) (a) Holm, R. H.; Kennepohl, P.; Solomon, E. I. *Chem. Rev.* **1996**, *96*, 2239–2314. (b) Beinert, H.; Holm, R. H.; Münck, E. *Science* **1997**, *277*, 653–659.
- (3) (a) Miller, J. S.; Drillon, M. *Magnetism: Molecules to Materials*; Wiley-VCH: Weinheim, 2001; Vols. 1–4. (b) Kahn, O. *Molecular Magnetism*; VCH: New York, 1993.
- (4) (a) Beckett, R.; Colton, R.; Hoskins, B. F.; Martin, R. L.; Vince, D. G. *Aust. J. Chem.* **1969**, *22*, 2527–2533. (b) Beckett, R.; Hoskins, B. F. *J. Chem. Soc., Dalton Trans.* **1972**, 291–295. (c) Ross, P. F.; Murmann, R. K.; Schlemper, E. O. *Acta Crystallogr.* **1974**, *B30*, 1120–1123. (d) Butcher, R. J.; O’Conner, C. J.; Sinn, E. *Inorg. Chem.* **1981**, *20*, 537–545. (e) Kwiatkowski, M.; Kwiatkowski, E.; Olechnowicz, A.; Ho, D. M.; Deutsch, E. *Inorg. Chim. Acta* **1988**, *150*, 65–73. (f) Bailey, N. A.; Fenton, D. E.; Moody, R.; Scrimshire, P. J.; Beloritzky, E.; Fries, P. H.; Latour, J.-M. *J. Chem. Soc., Dalton Trans.* **1988**, 2817–2824. (g) Agnus, Y.; Louis, R.; Metz, B.; Boudon, C.; Gisselbrecht, J. P.; Gross, M. *Inorg. Chem.* **1991**, *30*, 3155–3161. (h) Sakai, K.; Yamada, Y.; Tsubomura, T.; Yabuki, M.; Yamaguchi, M. *Inorg. Chem.* **1996**, *35*, 542–544. (i) Suh, M. P.; Han, M. Y.; Lee, J. H.; Min, K. S.; Hyeon, C. *J. Am. Chem. Soc.* **1998**, *120*, 3819–3820. (j) Wang, Y. Y.; Zhou, L. J.; Shi, Q.; Shi, Q. Z.; Gao, Y. C.; Hou, X. *Transition Met. Chem.* **2002**, *27*, 145–148. (k) Bian, H.-D.; Xu, J.-Y.; Gu, W.; Yan, S.-P.; Cheng, P.; Liao, D.-Z.; Jiang, Z.-H. *Polyhedron*, **2003**, *22*, 2927–2932.
- (5) (a) Hulsbergen, F. B.; ten Hoedt, R. W. M.; Verschoor, G. C.; Reedijk, J.; Spek, A. L. *J. Chem. Soc., Dalton Trans.* **1983**, 539–545. (b) Costes, J.-P.; Dahhan, F.; Laurent, J.-P. *Inorg. Chem.* **1986**, *25*, 413–416. (c) Angaroni, M.; Ardizzoia, G. A.; Beringhelli, T.; La Monica, G.; Gatteschi, D.; Masciocchi, N.; Moret, M. *J. Chem. Soc., Dalton Trans.* **1990**, 3305–3309. (d) Angaridis, P. A.; Baran, P.; Boča, R.; Cervantes-Lee, F.; Haase, W.; Mezei, G.; Raptis, R. G.; Werner, R. *Inorg. Chem.* **2002**, *41*, 2219–2228.

**Scheme 1.** (a)  $D_3$  Structure of TrisOH and (b) Coupling Scheme for a  $C_3$  Symmetric Trinuclear  $Cu^{II}$  Cluster (Top) and Its Energy Diagram When Antiferromagnetically Coupled (Bottom)



$= 1/2$  and  $3/2$ , and another  $S_{tot} = 1/2$  state, respectively. The two noninteracting  $S_{tot} = 1/2$  states are energetically degenerate, and

- (6) (a) Ferrer, S.; Lloret, F.; Bertomeu, I.; Alzueta, G.; Borrás, J.; García-Granda, S.; Liu-González, M.; Haasnoot, J. G. *Inorg. Chem.* **2002**, *41*, 5821–5830. (b) Ferrer, S.; Haasnoot, J. G.; Reedijk, J.; Müller, E.; Biagini Cingi, M.; Lanfranchi, M.; Manotti Lanfredi, A. M.; Ribas, J. *Inorg. Chem.* **2000**, *39*, 1859–1867.
- (7) Liu, X.; de Miranda, M. P.; McInnes, E. J. L.; Kilner, C. A.; Halcrow, M. A. *Dalton Trans.* **2004**, 59–64.
- (8) López-Sandoval, H.; Contreras, R.; Escuer, A.; Vicente, R.; Bernès, S.; Nöth, H.; Leigh, G. J.; Barba-Behrens, N. *J. Chem. Soc., Dalton Trans.* **2002**, 2648–2653.
- (9) (a) Kozłowski, M. C.; Li, X.; Carroll, P. J.; Xu, Z. *Organometallics* **2002**, *21*, 4513–4522. (b) Koderia, M.; Tachi, Y.; Kita, T.; Kobushi, H.; Sumi, Y.; Kano, K.; Shiro, M.; Koikawa, M.; Tokii, T.; Ohba, M.; Okawa, H. *Inorg. Chem.* **2000**, *39*, 226–234.
- (10) (a) Cage, B.; Cotton, F. A.; Dalal, N. S.; Hillard, E. A.; Rakvin, B.; Ramsey, C. M. *J. Am. Chem. Soc.* **2003**, *125*, 5270–5271. (b) Clérac, R.; Cotton, F. A.; Dunbar, K. R.; Hillard, E. A.; Petrukhnina, M. A.; Smucker, B. W. *C. R. Acad. Sci. Paris, Chimie/Chimie* **2001**, *4*, 315–319.
- (11) (a) Padilla, J.; Gatteschi, D.; Chaudhuri, P. *Inorg. Chim. Acta* **1997**, *260*, 217–220. (b) Chaudhuri, P.; Karpenstein, I.; Winter, M.; Butzlaff, C.; Bill, E.; Trautwein, A. X.; Flörke, U.; Haupt, H.-J. *J. Chem. Soc., Chem. Commun.* **1992**, 321–322.
- (12) Machonkin, T. E.; Mukherjee, P.; Henson, M. J.; Stack, T. D. P.; Solomon, E. I. *Inorg. Chim. Acta* **2002**, *341*, 39–44.
- (13) (a) Cole, A. P.; Root, D. E.; Mukherjee, P.; Solomon, E. I.; Stack, T. D. P. *Science* **1996**, *273*, 1848–1850. (b) Root, D. E.; Henson, M. J.; Machonkin, T.; Mukherjee, P.; Stack, T. D. P.; Solomon, E. I. *J. Am. Chem. Soc.* **1998**, *120*, 4982–4990.
- (14) (a) Solomon, E. I.; Chen, P.; Metz, M.; Lee, S.-K.; Palmer, A. E. *Angew. Chem., Int. Ed.* **2001**, *40*, 4570–4590. (b) Solomon, E. I.; Sundaram, U. M.; Machonkin, T. E. *Chem. Rev.* **1996**, *96*, 2563–2605. (c) Solomon, E. I.; Baldwin, M. J.; Lowery, M. D. *Chem. Rev.* **1992**, *92*, 521–542.
- (15) (a) Allendorf, M. D.; Spira, D. J.; Solomon, E. I. *Proc. Natl. Acad. Sci. U.S.A.* **1985**, *82*, 3063–3067. (b) Spira-Solomon, D. J.; Allendorf, M. D.; Solomon, E. I. *J. Am. Chem. Soc.* **1986**, *108*, 5318–5328. (c) Cole, J. L.; Tan, G. O.; Yang, E. K.; Hodgson, K. O.; Solomon, E. I. *J. Am. Chem. Soc.* **1990**, *112*, 2243–2249. (d) Shin, W.; Sundaram, U. M.; Cole, J. L.; Zhang, H. H.; Hedman, B.; Hodgson, K. O.; Solomon, E. I. *J. Am. Chem. Soc.* **1996**, *118*, 3202–3215. (e) Lee, S.-K.; George, S. D.; Antholine, W. E.; Hedman, B.; Hodgson, K. O.; Solomon, E. I. *J. Am. Chem. Soc.* **2002**, *124*, 6180–6193.
- (16) (a) Messerschmidt, A.; Ladenstein, R.; Huber, R.; Bolognesi, M.; Avigliano, L.; Petruzzelli, R.; Rossi, A.; Finazzi-Agró, A. *J. Mol. Biol.* **1992**, *224*, 179–205. (b) Messerschmidt, A.; Luecke, H.; Huber, R. *J. Mol. Biol.* **1993**, *230*, 997–1014. (c) Zaitseva, I.; Zaitsev, V.; Card, G.; Moshkov, K.; Bax, B.; Ralph, A.; Lindley, P. *J. Biol. Inorg. Chem.* **1996**, *1*, 15–23. (d) Zaitsev, V. N.; Zaitseva, I.; Papiz, M.; Lindley, P. F. *J. Biol. Inorg. Chem.* **1999**, *4*, 579–587. (e) Ducros, V.; Brzozowski, A. M.; Wilson, K. S.; Brown, S. H.; Østergaard, P.; Schneider, P.; Yaver, D. S.; Pedersen, A. H.; Davies, G. J. *Nat. Struct. Biol.* **1998**, *5*, 310–316. (f) Ducros, V.; Brzozowski, A. M.; Wilson, K. S.; Østergaard, P.; Schneider, P.; Svendsen, A.; Davies, G. J. *Acta Crystallogr.* **2001**, *D57*, 333–336. (g) Bertrand, T.; Jolivald, C.; Briozzo, P.; Caminade, E.; Joly, N.; Madzak, C.; Mougín, C. *Biochemistry* **2002**, *41*, 7325–7333. (h) Piontek, K.; Antorini, M.; Choinowski, T. *J. Biol. Chem.* **2002**, *277*, 37663–37669. (i) Hakulinen, N.; Kiiskinen, L.-L.; Kruus, K.; Saloheimo, M.; Paananen, A.; Koivula, A.; Rouvinen, J. *Nat. Struct. Biol.* **2002**, *9*, 601–605. (j) Roberts, S. A.; Weichsel, A.; Grass, G.; Thakali, K.; Hazzard, J. T.; Tollin, G.; Rensing, C.; Montfort, W. R. *Proc. Natl. Acad. Sci. U.S.A.* **2002**, *99*, 2766–2771. (k) Enguita, F. J.; Martins, L. O.; Henriques, A. O.; Carrondo, M. A. *J. Biol. Chem.* **2003**, *278*, 19416–19425.
- (17) Sinn, E. *Coord. Chem. Rev.* **1970**, *5*, 313–347.
- (18) (a) Griffith, J. S. *Struct. Bond.* **1972**, *10*, 87–126. (b) Kokoszka, G. F.; Duerst, R. W. *Coord. Chem. Rev.* **1970**, *5*, 209–244.

thus the trimer would be in either an antiferromagnetically coupled spin-frustrated (i.e., orbitally doubly degenerate  $S_{tot} = 1/2$ ) ground state or in a ferromagnetically coupled quartet ( $S_{tot} = 3/2$ ) state, separated by an energy of  $3J$ . From group theory, the quartet and two doublet states in  $D_3$  symmetry are  ${}^4A_2$  and  ${}^2E$ .<sup>19,20</sup> The  ${}^2E$  state can undergo spin-orbit coupling leading to a zero-field splitting into two Kramers doublets ( $\Gamma_4 + \Gamma_5, \Gamma_6$ ) split by  $\Delta$ .<sup>20–23</sup>

Studies on the EPR, optical, and Mössbauer spectra, as well as on the heat capacity and magnetic susceptibility of various polynuclear metal clusters, have demonstrated that the HDVV model is insufficient in explaining the observed data.<sup>20,24</sup> For example, low-temperature magnetic susceptibility studies of antiferromagnetically coupled  $Cu^{II}_3$  complexes have reported the anomalous decline of  $\chi_M T$  values below that expected for a one unpaired spin system.<sup>5–8</sup> Note that the expectation values calculated in these reports use the standard Van Vleck equation which employs the HDVV model that assumes Boltzmann population of noninteracting states.

Various interpretations of the unique properties of trimeric metal clusters all agree that the spin-frustration must be eliminated in the antiferromagnetically coupled ground state of these complexes. Within the framework of the HDVV model, static, dynamic, and magnetic Jahn–Teller effects have been proposed to account for the discrepancies from the HDVV model in the data.<sup>24</sup> Alternatively, so-called “non-Heisenberg coupling” effects, such as antisymmetric (= Dzialoshinsky–Moriya), anisotropic (= pseudo-dipolar), or biquadratic exchange, have been integrated into the HDVV Hamiltonian.<sup>20,24</sup>

In particular, antisymmetric exchange, introduced independently by Dzialoshinsky<sup>25</sup> and Moriya,<sup>26</sup> has been shown to be first-order in spin-orbit coupling in an exchange coupled system and has been suggested to be the largest non-Heisenberg term available, especially for trinuclear systems.<sup>20</sup> Considerable progress has been made in the theoretical predictions of the behavior of the  ${}^2E$  ground state of  $Cu^{II}_3$  clusters, by Tsukerblat and co-workers in particular.<sup>20–22</sup> Experimental applications of this exchange term have been reported for various  $Cu^{II}_3$  complexes<sup>6,7,11,22</sup> as well as for  $Fe^{III}_3$  and  $Cr^{III}_3$  carboxylates.<sup>23,27</sup> These studies, however, fall short of providing any direct spectroscopic proof and quantitation for the effects of antisymmetric exchange. Nevertheless, this exchange effect is now being applied to more complex systems. In bioinorganic chemistry, Münck and co-workers have employed antisymmetric exchange in the analysis of the unusual EPR and Mössbauer features

- (19) Tsukerblat, B. S. *Group Theory in Chemistry and Spectroscopy*; Academic Press: London, 1994.
- (20) Tsukerblat, B. S.; Belinskii, M. I.; Fainzil'berg, V. E. *Sov. Sci. Rev. B Chem.* **1987**, *9*, 337–481.
- (21) (a) Clemente, J. M.; Palií, A. V.; Tsukerblat, B. S.; Georges, R. In *Molecular Magnetism: From Molecular Assemblies to the Devices*; Coronado, E.; Delhaes, P.; Gatteschi, D.; Müller, J. S., Eds.; Kluwer: Dordrecht, 1996; pp 85–104. (b) Fainzil'berg, V. E.; Belinskii, M. I.; Kuyavskaya, B. Ya.; Tsukerblat, B. S. *Mol. Phys.* **1985**, *54*, 799–812. (c) Fainzil'berg, V. E.; Belinskii, M. I.; Tsukerblat, B. S. *Mol. Phys.* **1981**, *44*, 1195–1213. (d) Belinskii, M. I.; Tsukerblat, B. S.; Ablov, A. V. *Fiz. Tverd. Tela* **1974**, *16*, 989–999.
- (22) Tsukerblat, B. S.; Kuyavskaya, B. Ya.; Belinskii, M. I.; Ablov, A. V.; Novotortsev, V. M.; Kalinnikov, V. T. *Theor. Chim. Acta (Berl.)* **1975**, *38*, 131–138.
- (23) Rakitin, Yu. V.; Yablokov, Yu. V.; Zelentsov, V. V. *J. Magn. Reson.* **1981**, *43*, 288–301.
- (24) Cannon, R. D.; White, R. P. *Prog. Inorg. Chem.* **1988**, *36*, 195–298.
- (25) Dzialoshinsky, I. *J. Phys. Chem. Solids* **1958**, *4*, 241–255.
- (26) (a) Moriya, T. *Phys. Rev.* **1960**, *120*, 91–98. (b) Moriya, T. In *Magnetism*; Rado, G. T., Suhl, H., Eds.; Academic Press: New York, 1963; Vol. 1, pp 85–125.
- (27) Nishimura, H.; Date, M. *J. Phys. Soc. Jpn.* **1985**, *54*, 395–399.

displayed by the Fe clusters of methane monooxygenase, beef heart aconitase, and Rieske proteins.<sup>28</sup> Spectroscopic demonstration and characterization of this effect on a simple, high symmetry system is clearly desired.

To experimentally characterize the exchange interactions in a trimeric system, we have undertaken a detailed spectroscopic study of a tris( $\mu$ -hydroxy)tricopper(II) complex (= TrisOH) recently synthesized by Mirica and Stack.<sup>29</sup> The structure of TrisOH has been determined by X-ray crystallography at  $-130$  °C to have rigorous  $D_3$  symmetry (Scheme 1a). The magnetic susceptibility yields an isotropic exchange coupling constant of  $J \approx -105$  cm<sup>-1</sup>. As the closest distance between pairs of metal sites between trimers is 9.2 Å, the effect of intermolecular magnetic interaction should be negligible, and thus, the  $J$  obtained translates into the purely molecular doublet-quartet splitting energy of  $|3J| \approx 315$  cm<sup>-1</sup>.

TrisOH is ideal for elucidating the exchange interactions present in a trimeric system. First, the crystallographically imposed  $D_3$  symmetry of the complex allows the non-Heisenberg exchange interactions to be identified, particularly the antisymmetric exchange, without complications due to additional structural distortions. Second, symmetry lowering, suspected to be present in all trinuclear metal complexes,<sup>24,30,31</sup> can be readily quantified from deviations between the observed and calculated data for a symmetric system. Third, TrisOH is the simplest case of a strongly coupled trinuclear metal complex with one  $\mu_2$ -OH as the only bridging ligand between each metal pair, and the equivalence of these three bridging OH ligands makes it possible to simplify the ligand-field splittings and, in particular, the orbital superexchange pathways. Finally, the availability of single crystals with uniformly aligned molecular  $C_3$ -axes makes it experimentally feasible to study the anisotropy in the effective  $g$ -matrix of the ground state doublet.

This study presents direct experimental evidence for the existence of the competing effects of antisymmetric exchange and symmetry lowering. These include the spectroscopic observations of the zero-field splitting in the <sup>2</sup>E ground state of the trimer, the strong anisotropy of the effective  $g$ -value that can only be explained by the in-state spin-orbit coupling of the split <sup>2</sup>E state and the presence of an EPR transition which requires symmetry lowering. The results offer a specific account of the superexchange and antisymmetric exchange interactions with respect to the contributions of ground-to-ground and ground-to-excited state superexchange mechanisms.

## Experimental Section

Detailed descriptions of the synthesis, crystal structure, and magnetic susceptibility of TrisOH ([Cu<sub>3</sub>(DBED)<sub>3</sub>( $\mu$ -OH)<sub>3</sub>](ClO<sub>4</sub>)<sub>3</sub>, DBED = *N,N'*-di-*tert*-butylethylenediamine) are as reported.<sup>29</sup> The X-ray structure data were collected at a temperature of  $-130 \pm 1$  °C. TrisOH crystallizes in the  $R\bar{3}c$  (#167) space group with six trinuclear complexes per rhombo-

hedral (hexagonal axes) unit cell ( $a = 14.585(1)$  Å,  $c = 45.609(4)$  Å,  $V = 8402.4(1)$  Å<sup>3</sup>). An asymmetric unit contains one Cu, one hydroxide ligand, and one DBED ligand, which by symmetry forms a molecular structure with rigorous  $D_3$  symmetry. The 3-fold molecular  $C_3$ -axes are aligned with the  $c$ -axis of the unit cell. The closest distance between two copper centers of two trinuclear complexes is 9.2 Å, and the distance between the centers of neighboring molecules is 14.5 Å. No bridging ligand is present between the individual trimer molecules, and only the noncoordinating perchlorate counterions and possibly solvent molecule(s) are situated between the trimers. In addition, the magnetic susceptibility has indicated the ground state of TrisOH to be antiferromagnetically coupled with doublet-quartet splitting of  $\sim -315$  cm<sup>-1</sup>.

MCD spectra were collected with a Jasco J-810-150S spectropolarimeter operating with an S-20 photomultiplier tube and an Oxford SM4000-8T magnet. MCD spectra were measured at temperatures between 1.78 K and 120 K and fields between 0 T and  $\pm 7$  T and corrected for baseline effects. EPR spectra were obtained using a Bruker EMX spectrometer. For X-/Q-band experiments, Bruker ER 041XG/ER 051QR microwave bridges and ER 4102ST/ER 5106QT cavities were used, respectively. Temperatures from 3.5 to 150 K were maintained using an Oxford ITC503 temperature controller with an ESR 900 Continuous Flow Cryostat for X-band and a CF935 Dynamic Continuous Flow Cryostat for Q-band (transfer line GFS650 from Oxford Instruments).

The powder samples for both MCD and EPR experiments were prepared anaerobically by finely grinding the single crystals of TrisOH under a N<sub>2</sub> atmosphere in a glovebox. The mull samples were prepared by dispersing the powdered materials in poly(dimethylsiloxane) (Aldrich) or mineral oil (Mallinckrodt). For MCD experiments, the mull samples were uniformly spread between quartz disks (Heraeus-Amersil) and loaded into copper MCD cells and promptly frozen. For EPR experiments, the powder and mull samples were loaded into quartz EPR tubes (Wilmad) with outside diameter of either 4 mm (for X-band) or 2 mm (for Q-band). For single-crystal X-band EPR experiments, a crystal was mounted with a mulling agent (poly(dimethylsiloxane)) to the end of a quartz rod that fit snugly in a 4 mm EPR tube. The crystal was rotated around the three orthogonal laboratory axes,  $X$ ,  $Y$ , and  $Z$ , which (given the symmetry of the hexagonal space group) allowed the crystal to be oriented with the  $c$ -axis either parallel or perpendicular to the magnetic field.

DFT calculations were performed on IBM 3BT-RS/6000 workstations using the Amsterdam density functional (ADF) program, version 2002.03, developed by Baerends et al.<sup>32</sup> A triple- $\zeta$  Slater-type orbital basis set (ADF basis set TZP) with a single polarization function at the local density approximation of Vosko, Wilk, and Nusair<sup>33</sup> with nonlocal gradient corrections of Becke<sup>34</sup> and Perdew<sup>35</sup> were employed. The structural parameters were taken from the crystal structure of TrisOH. With truncation of the *tert*-butyl groups, the structure was optimized at  $C_3$  symmetry. The electronic structure of the ground

(28) (a) Tiago de Oliveira, F.; Bominaar, E. L.; Hirst, J.; Fee, J. A.; Münck, E. *J. Am. Chem. Soc.* **2004**, *126*, 5338–5339. (b) Sanakis, Y.; Macedo, A. L.; Moura, I.; Moura, J. J. G.; Papaefthymiou, V.; Münck, E. *J. Am. Chem. Soc.* **2000**, *122*, 11855–11863. (c) Kauffmann, K. E.; Popescu, C. V.; Dong, Y.; Lipscomb, J. D.; Que, L., Jr.; Münck, E. *J. Am. Chem. Soc.* **1998**, *120*, 8739–8746.

(29) Mirica, L. M.; Stack, T. D. P. Manuscript in preparation.

(30) Cannon, R. D.; Jayasooriya, U. A.; Sowrey, F. E.; Tilford, C.; Little, A.; Bourke, J. P.; Rogers, R. D.; Vincent, J. B.; Kearley, G. J. *Inorg. Chem.* **1998**, *37*, 5675–5677.

(31) Murao, T. *Phys. Lett.* **1974**, *49A*, 33–35.

(32) (a) Baerends, E. J.; Ellis, D. E.; Ros, P. *Chem. Phys.* **1973**, *2*, 41–51. (b) Te Velde, G.; Baerends, E. J. *J. Comput. Phys.* **1992**, *99*, 84–98.

(33) Vosko, S. H.; Wilk, L.; Nusair, M. *Can. J. Phys.* **1980**, *58*, 1200–1211.

(34) Becke, A. D. *J. Chem. Phys.* **1986**, *84*, 4524–4529.

(35) Perdew, J. P. *Phys. Rev. B* **1986**, *33*, 8822–8824.

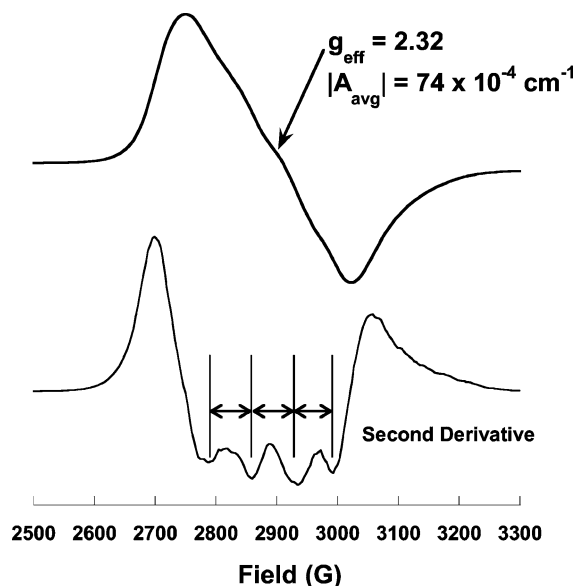


**Figure 1.** X-band EPR spectrum of powder TrisOH sample at 5 K, 9.39 GHz (top) and second derivative plot of the EPR spectrum (bottom). Four-line hyperfine splitting pattern is indicated.

$S_{\text{tot}} = 1/2$  state was calculated in the spin unrestricted broken symmetry state.<sup>36</sup>

## Results

The powder X-band ( $h\nu \sim 0.3 \text{ cm}^{-1}$ ) EPR spectrum of TrisOH taken at 5 K is presented in Figure 1 (top). Over the magnetic field range of 0 to 9000 G, one broad symmetric transition centered at 2890 G is observed, giving an effective  $g$ -value ( $g_{\text{eff}}$ ) of 2.32. The  $g_{\text{eff}}$  obtained at Q-band ( $h\nu \sim 1.1 \text{ cm}^{-1}$ , Figure S1) is very similar indicating that the ground state is an  $S = 1/2$  antiferromagnetically coupled trimer, consistent with the result from magnetic susceptibility.<sup>29</sup> Four hyperfine features with a small  $|A_{\parallel}|$  value of  $74 \times 10^{-4} \text{ cm}^{-1}$  are resolved from the second derivative plot shown in Figure 1 (bottom). The position and shape of this signal remain the same when the powder is frozen in a mulling agent as required for MCD experiments. The signal is strongly temperature dependent; it is only observed below  $\sim 30 \text{ K}$  and becomes more intense at lower temperatures (Figure S2). No additional feature is observed at temperatures up to 100 K.

Figure 2 inset shows the strong angular dependence of the transition in single-crystal X-band EPR experiments. The data were obtained at 3.7 K by rotating a TrisOH crystal around the three orthogonal laboratory  $X$ ,  $Y$ , and  $Z$  axes, with the  $Z$  axis parallel to the  $c$ -axis of the unit cell. The 3-fold molecular  $C_3$ -axis (i.e., molecular  $z$ -axis) is parallel, and the trimer plane (i.e., molecular  $x,y$ -axes) is perpendicular to the  $c$ -axis of the unit cell. Distinctly different sets of spectra were obtained with different orientations of the crystal: no signal is observed when the trimer plane is parallel to the applied field ( $H$ ), whereas a broad derivative shaped signal is observed when the molecular  $z$ -axis is parallel to  $H$  ( $\theta$  {angle between the  $C_3$ -axis and  $H$ } =  $0^\circ$ ). This latter signal is very similar in the resonance field and band shape to the powder pattern spectrum in Figure 1 with a similar hyperfine structure which quickly disappears as  $\theta$  is increased from  $0^\circ$ . As the molecular  $z$ -axis is rotated away from

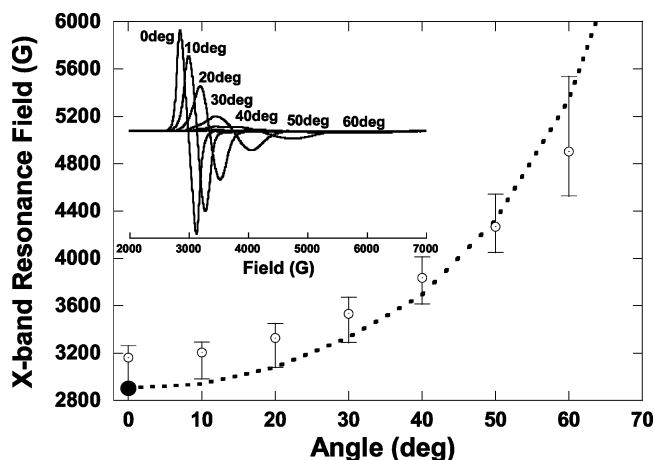


**Figure 2.** Resonance fields of the single-crystal TrisOH in X-band EPR. The horizontal axis of the plot defines the angle between the molecular  $z$ -axis (the 3-fold axis perpendicular to the  $\text{Cu}_3$  plane) relative to the applied magnetic field. Each point gives the average of five experiments (in open circles) and the high/low values (error bars). The resonance field of the powder EPR spectrum is indicated by the filled circle at  $0^\circ$ . Fits were made by varying the antisymmetric exchange ( $G$ ) and distortion factor ( $\delta$ ) as described in the text. The dotted curve represents the simulated angular dependence of the EPR transitions with the best fit values. (Inset) The overlay of the actual single-crystal EPR spectra at various angles.

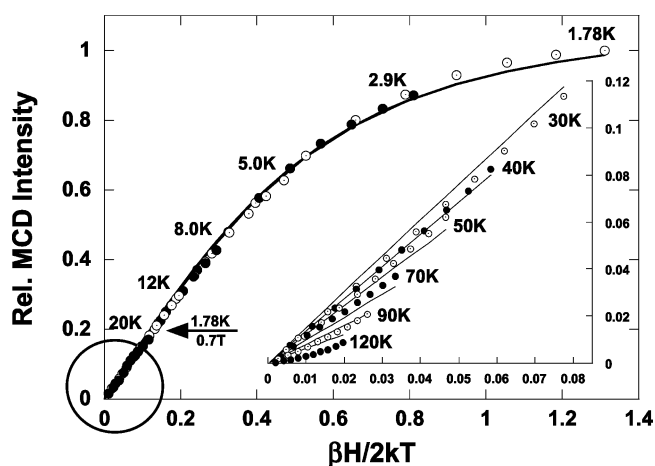


**Figure 3.** VTVH MCD of TrisOH (mull) at 330 nm. Twelve isotherms are shown (1.78, 2.9, 5.0, 8.0, 12, 20 K and 30, 40, 50, 70, 90, 120 K in the expanded scale of the circled region) with normalized intensities. Simulations were performed with two  $S = 1/2$  Kramers doublets, both with  $g_z = 2.32$ ,  $g_{xy}$ (effective) = 0, and equal C-term intensities ( $A_{\text{satim}}$ ) but with opposite signs. Contributions from A- and B-terms were ignored. Splitting between the two doublets, i.e.,  $\Delta = 65.0 \text{ cm}^{-1}$  is obtained. The arrow indicates 0.7 T in the 1.78 K isotherm (Figure 4).

the magnetic field ( $\theta > 0^\circ$ ), the observed transition strongly shifts toward a higher resonance field as shown in the Figure 2 inset. Between  $\theta = 0^\circ$  and  $60^\circ$ , the spectra span a wide range of resonance fields from 2910 G up to  $\sim 5540 \text{ G}$  which correspond to effective  $g$ -values of 2.31 down to  $\sim 1.2$ . With the increase of  $\theta$ , the EPR spectrum broadens and loses intensity; beyond  $\theta > 60^\circ$ , no transition is detectable due to further broadening and the fact that the resonance field exceeds the range of the instrument. Five sets of experiments were performed, and each point in Figure 2 shows the average and high/low values (error bars) of the acquired data.

Figure 3 shows VTVH MCD saturation isotherms of the mull sample between 1.78 and 120 K at 330 nm, which is the most intense MCD feature in the range of detection (2000 to 250

(36) Noodleman, L. *J. Chem. Phys.* **1981**, *74*, 5737–5743.

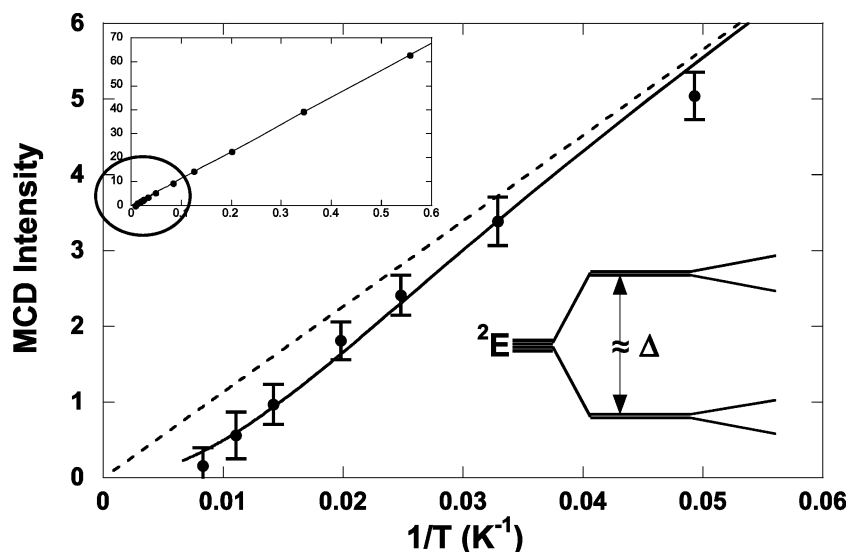


**Figure 4.**  $1/T$  plot of the MCD intensities at a fixed magnetic field of 0.7 T. Data points were collected over 12 temperatures between 1.78 and 120 K (see Figure 3). The main panel shows data points between 20 and 120 K, which is the expanded view of the circled region in the inset. The simulation assumed two level Boltzmann distribution with each state having MCD C-terms with the same magnitude but with opposite signs (solid line). The linear  $1/T$  dependence of one-level systems (i.e. infinite  $\Delta$  limit in the two level systems) is shown in the dotted line for comparison.

nm).<sup>37</sup> The data have been normalized and plotted vs  $\beta H/2kT$ .<sup>38–40</sup> No nesting behavior (i.e., lack of overlap between the saturation curves obtained at different temperatures<sup>38–40</sup>) is present in the low-temperature range between 1.78 and 20 K, as expected for a typical  $S = 1/2$  spin system. However, a distinct nesting behavior is observed at higher temperatures ( $> 30$  K). An increase of temperature causes a reduction of the relative MCD intensities and a gradual decrease of the slope of the isotherms (Figure 3, expanded scale). In addition, the saturation curves at all temperatures deviate significantly from the simple  $S = 1/2$  Brillouin Curve<sup>3b</sup> (Figure S3) with a smaller slope, which suggests strong anisotropy of the  $g$ -matrix yielding an average  $g$ -value that is significantly smaller than the  $g$ -factor of the free electron ( $= 2.0023$ ).

Figure 4 plots the relative MCD intensities obtained over the temperature range 1.78 K to 120 K in a fixed applied magnetic field (0.7 T) in which no saturation of the MCD intensity occurs (the 1.78 K, 0.7 T point indicated by the arrow in Figure 3). At temperatures above 20 K, the linear dependence of the MCD intensity on  $1/T$  is gradually lost, indicating population of an excited state as described in the following section.

## Analysis

### 1. Zero-Field Splitting of the Ground ${}^2E$ State of TrisOH and Direct Evidence of the Low-Lying $S = 1/2$ Excited State.

The total MCD intensity of an  $S = 1/2$  ground state (in the nonsaturating limit of  $kT > g\beta H$ ) can be expressed as:<sup>41,42</sup>

$$\frac{\Delta\epsilon}{E} = \gamma\beta H \left[ \left( -\frac{\partial f(E)}{\partial E} \right) A_1 + \left( B_0 + \frac{C_0}{kT} \right) f(E) \right] \quad (1)$$

where  $\gamma$  is a collection of constants,  $\beta$  is the Bohr magneton,  $k$

is the Boltzmann constant,  $T$  is the absolute temperature,  $H$  is the external magnetic field,  $f(E)$  is the line shape function, and  $E$  is the energy of the incident radiation. The three terms are referred to as the A-, B-, and C-terms, respectively, and all are linear in  $H$ . In particular, the C-term ( $C_0/kT$ ) derives from the differential population between Zeeman-split subcomponents of the  $S = 1/2$  Kramers doublet and is proportional to  $1/T$  in the nonsaturating linear limit ( $kT > g\beta H$ ). This term dominates the MCD intensity for a paramagnetic system being several orders of magnitude larger than the other terms at low temperatures.

The deviation of the MCD intensity from the linear dependence on  $1/T$  (Figure 4), therefore, requires involvement of more than one  $S = 1/2$  state. Thus, this is direct evidence of the low-lying excited  $S = 1/2$  state originating from the removal of the degeneracy of the spin frustrated  ${}^2E$  ground state of the trimeric  $\text{Cu}^{II}_3$  cluster. In the 3-fold symmetric ( $C_3$ ) limit, these two  $S_{\text{tot}} = 1/2$  states derive from the spin-orbit coupling within the  ${}^2E$  state and are associated with orbital angular momenta of opposite signs ( $L_z = \pm 1$ ).<sup>21a</sup> Therefore, equal but oppositely signed MCD C-terms are expected. Using the two-state Boltzmann distribution, the energy separation between the two states can be obtained from the following equation describing the total MCD intensity at a fixed wavelength  $\lambda$  as a function of temperature  $T$ :

$$I_{\text{MCD}}(\lambda) = \frac{C}{T} \frac{1 - \exp\left(-\frac{\Delta hc}{kT}\right)}{1 + \exp\left(-\frac{\Delta hc}{kT}\right)} \quad (2)$$

where  $C$  is the MCD intensity of the ground  $S = 1/2$  state,  $\Delta$  is

(37) A detailed study of the excited-state MCD spectrum of TrisOH is in progress.

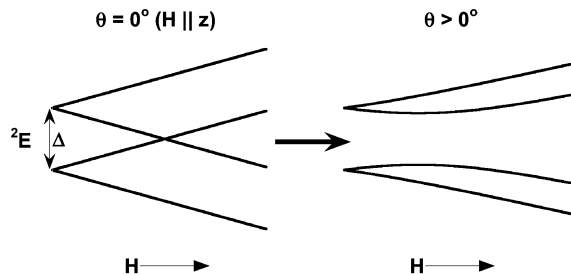
(38) Solomon, E. I.; Hanson, M. A. In *Inorganic Electronic Structure and Spectroscopy*; Solomon, E. I., Lever, A. B. P., Eds.; John Wiley & Sons: New York, 1999; pp 1–129.

(39) Solomon, E. I.; Pavel, E. G.; Loeb, K. E.; Campochiaro, C. *Coord. Chem. Rev.* **1995**, *144*, 369–460.

(40) (a) Solomon, E. I.; Brunold, T. C.; Davis, M. I.; Kemsley, J. N.; Lee, S.-K.; Lehnert, N.; Neese, F.; Skulan, A. J.; Yang, Y.-S.; Zhou, J. *Chem. Rev.* **2000**, *100*, 235–349. (b) Solomon, E. I.; Decker, A.; Lehnert, N. *Proc. Natl. Acad. Sci. U.S.A.* **2003**, *100*, 3589–3594. (c) Solomon, E. I. *Inorg. Chem.* **2001**, *40*, 3656–3669.

(41) Neese, F.; Solomon, E. I. *Inorg. Chem.* **1999**, *38*, 1847–1865.

(42) (a) Stephens, P. J. *Annu. Rev. Phys. Chem.* **1974**, *25*, 201–232. (b) Piepho, S. B.; Schatz, P. N. *Group Theory in Spectroscopy with Applications to Magnetic Circular Dichroism*; John Wiley & Sons: New York, 1983.

**Scheme 2.** Angular Dependence of the Zeeman Splitting of the Zero-Field Split  $^2E$  Ground State of a Trinuclear  $\text{Cu}^{\text{II}}$  Cluster

the energy difference between this ground and the excited  $S = 1/2$  states (i.e., the  $^2E$  zero-field splitting),  $h$  is Planck's constant ( $6.626 \times 10^{-34}$  J s),  $c$  is the speed of light ( $2.998 \times 10^{10}$  cm  $s^{-1}$ ),  $k$  is Boltzmann's constant ( $1.38 \times 10^{-23}$  J  $K^{-1}$ ), and  $T$  is the temperature in Kelvin. The best fit to the data in Figure 4, on varying  $C$  and  $\Delta$ , was achieved with  $\Delta = 67.2 \pm 2.9$   $\text{cm}^{-1}$ .

For a more comprehensive description of the MCD intensity, the VTVH MCD saturation magnetization isotherms (1.78 K to 120 K in Figure 3) were simulated with the MCD C-term orientation averaged intensity expression:<sup>39,43</sup>

$$\Delta\epsilon = \sum_i (A_{\text{satlim}})_i \left\{ \int_0^{(\pi/2)} \frac{\cos^2\theta \sin\theta}{\Gamma_i} (g_{\parallel i}) \alpha_i d\theta - \sqrt{2} \frac{M_z}{M_{xy}} \int_0^{(\pi/2)} \frac{\sin^3\theta}{\Gamma_i} (g_{\perp i}) \alpha_i d\theta \right\} \quad (3)$$

where

$$\Gamma_i = \sqrt{(g_{\parallel i} \cos\theta)^2 + (g_{\perp i} \sin\theta)^2} \quad (4)$$

$$\alpha_i = \frac{e^{-(E_i - \Gamma_i \beta H / kT)} - e^{-(E_i + \Gamma_i \beta H / kT)}}{\sum_j e^{-(E_j - \Gamma_j \beta H / kT)} + e^{-(E_j + \Gamma_j \beta H / kT)}} \quad (5)$$

$\theta$  is the angle between the magnetic field and the molecular  $z$ -axis,  $(A_{\text{satlim}})_i$  is the C-term intensity scaling factor,  $E_i$  is the relative energy of each  $S = 1/2$  state (i.e.,  $E_0 = 0$  and  $E_1 = \Delta$ , the zero-field splitting), and  $\alpha_i$  is the Boltzmann population term.

The 330 nm band in the absorption and MCD spectra is a  $\mu_2\text{-OH}^-$  to  $\text{Cu}^{\text{II}}$  charge-transfer transition.<sup>37</sup> The in- $\text{Cu}_3$  plane positions of the O ligands require this charge-transfer transition to be polarized along the  $x,y$ -directions. The  $x,y$ -polarized transitions acquire MCD intensity when the magnetic field is along the molecular  $z$ -axis, and at this orientation, the two  $S = 1/2$  components of the zero-field split  $^2E$  ground state can be described by two unperturbed Kramers doublets with equal  $g$ -values (vide infra) as depicted in Scheme 2 (left). Accordingly, two isolated Kramers doublets, separated by  $\Delta$ , were included in the simulation of the VTVH MCD data shown in Figure 3, using eq 3. Simulations were performed by varying  $E_1 = \Delta$  and  $(A_{\text{satlim}})_1 = -(A_{\text{satlim}})_0$ , with a fixed value of  $g_{\parallel i}$  (= effective  $g_z$ ) at 2.32 (from the EPR experiments);  $g_{\perp i}$  (= effective  $g_{x,y}$ ) and the polarization ratio  $M_z/M_{xy}$  were both set equal to zero, the former from the angular dependence of the single-crystal

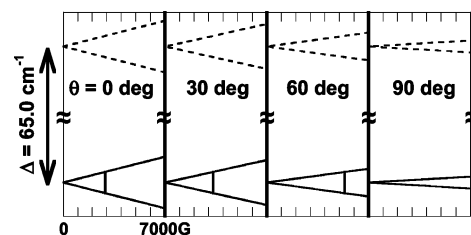


**Figure 5.** Zeeman splitting energy diagrams of the two Kramers doublets at four different orientations relative to the applied magnetic field. Diagrams are plotted to scale (except for the relative energy between the upper and lower doublets), with magnetic fields up to 7000 G, the upper limit of observed transitions in the experiments. The lengths of the vertical lines are the energy of the X-band radiation ( $0.3$   $\text{cm}^{-1}$ ). The field positions of these vertical lines depict where the actual transitions occur at each molecular orientation.

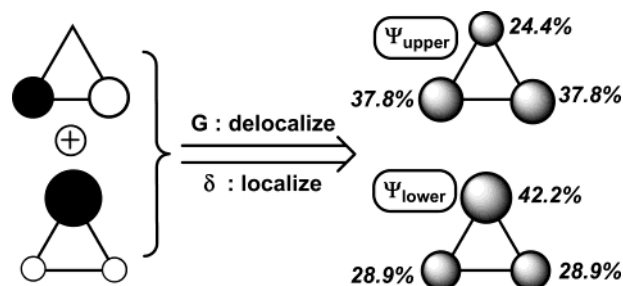


**Figure 6.** Spin density of the two doublets split from the ground  $^2E$  state. On the left is the schematic description of the basis spin wave functions (eqs 7–10). On the right are the spin densities on each Cu site,  $\Psi_{\text{lower}}$  being the ground state and  $\Psi_{\text{upper}}$  being the excited state.

EPR spectra (vide infra) and the latter from the fact that the 330 nm transition is  $x,y$  polarized. The simulated VTVH MCD curves are given as solid lines in both the main panel and inset of Figure 3. The best fit was achieved with a zero-field splitting  $\Delta$  of the  $^2E$  of  $65$   $\text{cm}^{-1}$ , in excellent agreement with the VT MCD simulation in Figure 4.

**2. Contributions to the Zero-Field Splitting: Antisymmetric Exchange and Symmetry Lowering.** To explain the unusually strong anisotropy of the effective  $g$ -values in the single-crystal EPR data of  $\text{TrisOH}$  in Figure 2, the spin Hamiltonian in eq 6 for a trigonal  $\text{Cu}_3^{\text{II}}$  system was implemented. This Hamiltonian accounts for antisymmetric exchange and symmetry lowering (from  $C_3$ ) in the structure.<sup>20–23</sup>

$$\hat{H} = -2J(\hat{S}_1 \cdot \hat{S}_2 + \hat{S}_2 \cdot \hat{S}_3 + \hat{S}_1 \cdot \hat{S}_3) + \delta(\hat{S}_1 \cdot \hat{S}_2) + \delta'(\hat{S}_1 \cdot \hat{S}_3) + \mathbf{G}([\hat{S}_1 \times \hat{S}_2] + [\hat{S}_2 \times \hat{S}_3] + [\hat{S}_3 \times \hat{S}_1]) + (g_z \cos\theta + g_{xy} \sin\theta)\beta H(\hat{S}_1 + \hat{S}_2 + \hat{S}_3) \quad (6)$$

where  $J$  is the isotropic exchange parameter,  $\delta$  and  $\delta'$  are the small changes in the isotropic exchange due to symmetry lowering, and  $\mathbf{G}$  is the antisymmetric exchange vector parameter for two-center interactions. In trigonal systems, the components of  $\mathbf{G}$  are assumed to follow the relation  $G_z \gg (G_x, G_y) \approx 0$  ( $z$  being the 3-fold axis), which can be derived from the symmetry properties of the  $\mathbf{G}$  vector.<sup>26,44</sup> With the following spin basis wave functions  $|\mathcal{S}', S_{\text{tot}}, M_S\rangle$  for a trinuclear  $\text{Cu}_3^{\text{II}}$ , with  $S_1 = S_2$

(44) Each metal pair in  $\text{TrisOH}$  has a 2-fold rotation axis passing through the midpoint of the pair, and the axis is in the  $\text{Cu}_3$  plane. The symmetry rules of the  $\mathbf{G}$  vectors allow the nonzero  $G$  component to be oriented perpendicular to the 2-fold axis. The collection of these components from the three metal pairs results in  $G_z \neq 0$  and  $(G_x, G_y) \approx 0$ .

(43) Pavel, E. G.; Kitajima, N.; Solomon, E. I. *J. Am. Chem. Soc.* **1998**, *120*, 3949–3962.

$= S_3 = 1/2$  (the intermediate spin state  $S' = S_2 + S_3$  and the total spin state  $S_{\text{tot}} = S_1 + S'$ ),<sup>45</sup>

$$\left|0, \frac{1}{2}, +\frac{1}{2}\right\rangle = \frac{1}{\sqrt{2}}\left(\left|\frac{1}{2}, -\frac{1}{2}, \frac{1}{2}\right\rangle - \left|\frac{1}{2}, \frac{1}{2}, -\frac{1}{2}\right\rangle\right) \quad (7)$$

$$\left|0, \frac{1}{2}, -\frac{1}{2}\right\rangle = \frac{1}{\sqrt{2}}\left(\left|-\frac{1}{2}, -\frac{1}{2}, \frac{1}{2}\right\rangle - \left|-\frac{1}{2}, \frac{1}{2}, -\frac{1}{2}\right\rangle\right) \quad (8)$$

$$\left|1, \frac{1}{2}, +\frac{1}{2}\right\rangle = \frac{1}{\sqrt{6}}\left(2\left|\frac{1}{2}, -\frac{1}{2}, \frac{1}{2}\right\rangle - \left|\frac{1}{2}, -\frac{1}{2}, -\frac{1}{2}\right\rangle - \left|\frac{1}{2}, \frac{1}{2}, -\frac{1}{2}\right\rangle\right) \quad (9)$$

$$\left|1, \frac{1}{2}, -\frac{1}{2}\right\rangle = \frac{1}{\sqrt{6}}\left(-2\left|\frac{1}{2}, -\frac{1}{2}, \frac{1}{2}\right\rangle + \left|-\frac{1}{2}, \frac{1}{2}, -\frac{1}{2}\right\rangle + \left|-\frac{1}{2}, -\frac{1}{2}, \frac{1}{2}\right\rangle\right) \quad (10)$$

the eigenvalues and eigenfunctions have been derived<sup>20–23</sup> for the two zero-field plus Zeeman split doublets of the <sup>2</sup>E state as

$$E_{\text{lower}}^{\pm} = -\frac{1}{2}(\Delta^2 + g^2\beta^2H^2 \mp 2\beta H(g^2\delta^2 + 3G^2g_z^2\cos^2\theta)^{1/2}) \quad (11)$$

$$E_{\text{upper}}^{\pm} = +\frac{1}{2}(\Delta^2 + g^2\beta^2H^2 \pm 2\beta H(g^2\delta^2 + 3G^2g_z^2\cos^2\theta)^{1/2}) \quad (12)$$

$$\Psi_{\text{lower}}^{\pm} = \sqrt{\frac{1}{2}\left(1 + \frac{\delta}{\Delta}\right)}\left|1, \frac{1}{2}, \pm\frac{1}{2}\right\rangle \pm i\sqrt{\frac{1}{2}\left(1 - \frac{\delta}{\Delta}\right)}\left|0, \frac{1}{2}, \pm\frac{1}{2}\right\rangle \quad (13)$$

$$\Psi_{\text{upper}}^{\pm} = \sqrt{\frac{1}{2}\left(1 - \frac{\delta}{\Delta}\right)}\left|1, \frac{1}{2}, \pm\frac{1}{2}\right\rangle \mp i\sqrt{\frac{1}{2}\left(1 + \frac{\delta}{\Delta}\right)}\left|0, \frac{1}{2}, \pm\frac{1}{2}\right\rangle \quad (14)$$

where the zero-field splitting is

$$\Delta = \sqrt{\delta^2 + 3G^2} \quad (15)$$

The subscripts *lower* and *upper* refer to the lower and higher energy  $S = 1/2$  doublets, respectively, and the + and – signs refer to the higher and lower energy Zeeman levels within each doublet, respectively.  $G = G_z$ ,  $g' = \sqrt{(g_z\cos\theta)^2 + (g_{x,y}\sin\theta)^2}$  where  $g_z$  and  $g_{x,y}$  are the real  $g$  values and  $\delta' \approx \delta$  and  $(G_x, G_y) \approx 0$  are assumed. Sketches of the energy levels at  $\theta = 0^\circ$  and  $\theta \neq 0^\circ$  are presented in Scheme 2.<sup>46</sup> Note that for  $\theta = 0^\circ$ , two isolated doublets split by  $g_z$ , whereas for  $\theta > 0^\circ$ , the off-diagonal matrix elements between these doublets result in nonlinear dependence on  $H$  and small effective  $g_{x,y}$  values. If  $\delta = 0$  is assumed, which would be the case for the trigonal structure determined from crystallography,  $\Delta$  would equal  $\sqrt{3}G$ . Therefore,  $G = 37.5 \text{ cm}^{-1}$  would be obtained from the  $\Delta$  estimated by VTVH MCD.

(45)  $|1, 3/2, \pm 3/2\rangle$  and  $|1, 3/2, \pm 1/2\rangle$  can be similarly obtained to describe the  $S_{\text{tot}} = 3/2$  state. It has been shown that the  $S_{\text{tot}} = 3/2$  state is not perturbed by the antisymmetric exchange term,  $G$ , and does not affect the description of the  $S_{\text{tot}} = 1/2$  states.

(46) The Zeeman energy levels are linearly dependent on  $H$  only when  $\theta = 0^\circ$  (Scheme 2 (left)). At this limit, the nonnesting behavior would be expected in VTVH MCD, which is the case for TrisOH in the low-temperature region (1.78 to 20 K). If  $\theta \neq 0^\circ$ , nesting would be observed even at this low-temperature region. Thus, the assignment of the 330 nm band as  $x,y$ -polarized is validated.

However, with the relatively large zero-field splitting ( $\Delta$ ) of  $65 \text{ cm}^{-1}$ , the only possible EPR transition that can occur in X- or Q-band is between the Zeeman subcomponents of the lower Kramers doublet in Scheme 2 (left); the upper doublet lacks population at low temperatures. For  $\theta = 0^\circ$ , these transitions are allowed only if  $\delta \neq 0$ , as the transition probability at the  $H_{\parallel}$   $z$  orientation is described by the following expression where the wave functions are given in eq 13.

$$|\langle\Psi_{\text{lower}}^+|\hat{S}_+ + \hat{S}_-|\Psi_{\text{lower}}^-\rangle|^2 \propto \delta^2/\Delta^2 \quad (16)$$

Therefore, the existence of an observable EPR intensity at  $\theta = 0^\circ$  for TrisOH in Figures 1 and 2 requires symmetry lowering of the geometry of the TrisOH complex (i.e.,  $\delta \neq 0$ ), despite its rigorous 3-fold symmetry required by crystallography.

Simulations were thus performed by considering an equilateral to isosceles distortion with  $\delta = \delta'$ . The single-crystal EPR resonance fields at different angles ( $\theta$ ) were simulated with a range of  $\delta$ 's by matching the X-band energy ( $0.313 \text{ cm}^{-1}$ ) to the energy differences of the two Zeeman sublevels given in eq 11. All data points from the single-crystal EPR experiments were taken into account; the  $g_z$  was fixed at 2.32, which was obtained from both the powder and  $\theta = 0^\circ$  single-crystal EPR data. The value of  $g_{x,y}$  of 2.0 was chosen after several initial trials to match the experiment; small variations in  $g_{x,y}$  ( $\Delta g_{x,y} = \pm 0.1$ ) were found to have a negligible influence on the energy levels.

The best fit to the data in Figure 2 was obtained with  $\delta = 17.5 \pm 5.0 \text{ cm}^{-1}$ , thus confirming symmetry lowering of TrisOH at low temperatures. Using eq 15 and  $\Delta = 65.0 \text{ cm}^{-1}$ ,  $G$  of  $36.0 \pm 0.8 \text{ cm}^{-1}$  is obtained. This is only  $\sim 1.5 \text{ cm}^{-1}$  different from the value obtained for the  $\delta = 0$  case ( $37.5 \text{ cm}^{-1}$ , vide supra), suggesting that when  $G$  is large, it is not very sensitive to  $\delta$ . The dotted line in Figure 2 has been simulated with these final parameter values. Figure 5 depicts how the energy levels change at different  $\theta$  and where the X-band transitions occur (solid vertical lines).

Given the experimental values of  $\Delta$  and  $\delta$ , a quantitative description of the spin wave functions is accessible. Substituting  $\delta = 17.5 \text{ cm}^{-1}$  and  $\Delta = 65 \text{ cm}^{-1}$  to eqs 13 and 14 gives

$$\Psi_{\text{lower}}^{\pm} = (0.797)\left|1, \frac{1}{2}, \pm\frac{1}{2}\right\rangle \pm (0.605)i\left|0, \frac{1}{2}, \pm\frac{1}{2}\right\rangle \quad (17)$$

$$\Psi_{\text{upper}}^{\pm} = (0.605)\left|1, \frac{1}{2}, \pm\frac{1}{2}\right\rangle \mp (0.797)i\left|0, \frac{1}{2}, \pm\frac{1}{2}\right\rangle \quad (18)$$

Symmetry lowering ( $\delta \neq 0$ ) concentrates more spin density on one metal site in the lower doublet ( $\Psi_{\text{lower}}^{\pm}$ ) and on the other two metal sites in the upper doublet ( $\Psi_{\text{upper}}^{\pm}$ ) (Figure 6). The spin densities on each metal site can be calculated from eq 7 to 10 and eq 13, 14. As a result, the spin density is distributed  $42 \pm 3\%$ ,  $29 \pm 1\%$ , and  $29 \pm 1\%$  over the three  $\text{Cu}^{\text{II}}$  sites in the lower doublet (i.e., the ground  $S = 1/2$  state) and  $24 \pm 3\%$ ,  $38 \pm 1\%$ ,  $38 \pm 1\%$  in the upper doublet, all deviating from the spin density of 33.3% in a totally delocalized trimeric system.

The hyperfine splittings in the powder X-band EPR spectrum would arise from the combined contributions from all of the metal sites.<sup>47</sup> With the spin density distributions obtained above, simulations were performed using four sets of standard Gaussian

(47) Belinsky, M. I. *Inorg. Chem.* **2004**, *43*, 739–746.

functions, each set comprised of seven Gaussian functions with relative intensities of 1:2:3:4:3:2:1; thus, there is a total of 28 hyperfine lines (Figures S4, S5). The relative positions of the four sets are the hyperfine splitting due to the unique metal center with 42% spin density, and the seven line pattern within each set are the combined hyperfine splitting due to the other two equivalent metal centers each with 29% spin density. Both the data and the simulation show four minima in the second derivative plots near the center of the band envelope. In the simulation, the positions of the minima are very similar to the positions of four hyperfine lines of the unique metal center; the small shifts in positions are caused by the contributions from the other metal hyperfine lines. Thus, it can be estimated that the observed hyperfine splitting ( $|A_{\text{avg}}| = 74 \times 10^{-4} \text{ cm}^{-1}$ ) is about 42% of the  $|A_{ij}|$  value of an isolated  $\text{Cu}^{\text{II}}$  site. Scaling up the observed value by 2.4 ( $= 100/42$ ) yields  $180 \times 10^{-4} \text{ cm}^{-1}$ , which is reasonable for a typical Cu parallel hyperfine splitting.

In summary, the low-lying excited  $S = 1/2$  state of a trinuclear metal cluster has been directly identified with a consistent zero-field splitting energy value ( $\Delta$ ), using VT MCD and VTVH MCD; antisymmetric exchange has been successfully implemented in the analysis of the strong anisotropy of the single-crystal EPR signals and found to be large; a lowering of the crystallographic  $D_3$  symmetry is required by the data. The competing effects of delocalization due to antisymmetric exchange ( $G$ ) and localization due to symmetry lowering ( $\delta$ ) result in a significant reduction of the observed parallel hyperfine splitting.

**3. Orbital Origin of Antisymmetric Exchange.** The orbital origin of the large antisymmetric exchange interaction of  $\sim 36 \text{ cm}^{-1}$  can be seen by evaluating the specific spin-orbit coupling pathways between each pair of metal centers. The formalism of the antisymmetric exchange is derived from second-order perturbation theory.<sup>26</sup> Approximating the orbital ground state on each metal site in TrisOH to be  $d_{x^2-y^2}$ , we can describe the vector component  $G_z$  between metals 1 and 2 (indicated  $G_z^{12}$ ) by the following expression:<sup>26,48</sup>

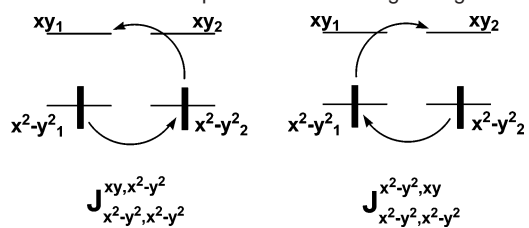
$$G_z^{12} = 2i\lambda \left[ \frac{\langle x^2 - y^2_1 | L_{1z} | xy_1 \rangle}{E_{x^2-y^2_1}^{xy}} (-2J_{x^2-y^2_1, x^2-y^2_2}^{xy, x^2-y^2_2}) - \frac{\langle x^2 - y^2_2 | L_{2z} | xy_2 \rangle}{E_{x^2-y^2_2}^{xy}} (-2J_{x^2-y^2_2, x^2-y^2_1}^{x^2-y^2_1, xy_1}) \right] \quad (19)$$

where the  $\lambda$  is the spin-orbit coupling parameter,  $L_{iz}$  is the orbital angular momentum operator, and  $E_{x^2-y^2_i}^{xy}$  is the energy difference between the ground  $d_{x^2-y^2_i}$  state (denoted  $x^2-y^2_i$ ) and the excited  $d_{xy_i}$  state (denoted  $xy_i$ ), where  $i$  indicates the metal site. The exchange integrals  $J_{x^2-y^2_1, x^2-y^2_2}^{xy, x^2-y^2_2}$  and  $J_{x^2-y^2_2, x^2-y^2_1}^{x^2-y^2_1, xy_1}$  can be explicitly written as

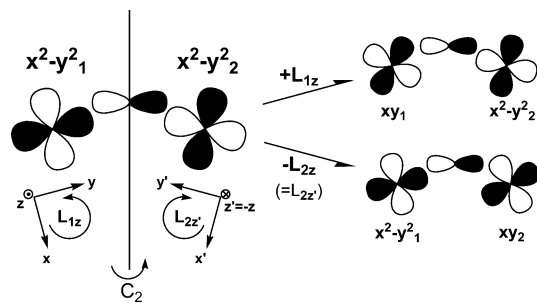
$$J_{x^2-y^2_1, x^2-y^2_2}^{xy, x^2-y^2_2} = \left\langle x^2 - y^2_1(1) x^2 - y^2_2(2) \left| \frac{e^2}{r_{12}} \right| xy_1(2) x^2 - y^2_2(1) \right\rangle \quad (20)$$

$$J_{x^2-y^2_2, x^2-y^2_1}^{x^2-y^2_1, xy_1} = \left\langle x^2 - y^2_1(1) x^2 - y^2_2(2) \left| \frac{e^2}{r_{12}} \right| x^2 - y^2_1(2) xy_2(1) \right\rangle \quad (21)$$

**Scheme 3.** Pictorial Description of the Exchange Integrals



**Scheme 4.** Spin-Orbit Coupling in a Metal Pair of TrisOH Bridged by an Oxygen Ligand<sup>a</sup>



<sup>a</sup> The orbital angular momentum operators  $L_{1z}$  and  $L_{2z'}$  ( $= -L_{2z}$ ) and their relative signs are described, in which the non-primed axes ( $x, y, z$ ) refer to the metal 1 coordinate system and the primed axes ( $x', y', z'$ ) refer to the metal 2, both being in the right-handed system. The orbitals are positioned to correspond to the crystal structure of TrisOH, with a Cu-O-Cu angle of  $144.2^\circ$  and  $x^2 - y^2_2$  rotated  $120^\circ$  with respect to  $x^2 - y^2_1$ .

where 1 and 2 in the parentheses refer to electrons. For example,  $J_{x^2-y^2_1, x^2-y^2_2}^{xy, x^2-y^2_2}$  involves transfer of the electron in the ground  $x^2 - y^2$  orbital state of the first metal to the ground  $x^2 - y^2$  state of the second, while the electron in the ground  $x^2 - y^2$  state of the second metal is transferred to the excited  $xy$  orbital state of the first (Scheme 3 (left)).<sup>49</sup>

In Scheme 4, the point group symmetry operation ( $C_2$ ) of each metal pair in the trimer and the associated axes are shown, with the nonprimed axes ( $x, y, z$ ) belonging to metal 1 and the primed axes ( $x', y', z'$ ) belonging to metal 2. Scheme 4 (left) shows the antibonding molecular orbital with each metal in its ground  $x^2 - y^2$  state. Scheme 4 (right) shows the molecular orbital obtained upon rotating one of the  $x^2 - y^2$  orbitals into an  $xy$  orbital, via the orbital angular momentum operators  $L_{1z}$  (top) or  $L_{2z'}$  (bottom). The directions of these operators follow the right-handed rule. In addition, note that the phases of the d-orbitals are determined by their antibonding interactions with the bridging oxygen p-orbital. At both metal sites,  $x^2 - y^2$  to  $xy$  transformations have positive overlap upon rotational operations by  $L_{1z}$  and  $L_{2z'}$ . However,  $z = -z'$ , and therefore,  $L_{2z} = -L_{2z'}$ . Thus, eq 19 can be simplified as

$$G_z^{12} = 4i\lambda \frac{\langle x^2 - y^2_2 | L_{2z} | xy_2 \rangle}{E_{x^2-y^2_2}^{xy}} (-2J_{x^2-y^2_2, x^2-y^2_1}^{xy, x^2-y^2_1}) \quad (22)$$

since  $\langle x^2 - y^2_2 | L_{2z} | xy_2 \rangle = -\langle x^2 - y^2_1 | L_{1z} | xy_1 \rangle$ . Note that, in metal dimers with a center of inversion,  $L_{2z'}$  equals  $+L_{2z}$  as the coordinate system on the metal 2 becomes left-handed (Scheme

(48) (a) Gatteschi, D.; Bencini, A. In *Magneto-Structural Correlations in Exchange Coupled Systems*; Willett, R. D., Gatteschi, D., Kahn, O., Eds.; D. Reidel: Dordrecht, The Netherlands, 1985; pp 241–268. (b) Bencini, A.; Gatteschi, D. *Electron Paramagnetic Resonance of Exchange Coupled Systems*; Springer-Verlag: Berlin, 1990.

(49) Since  $(G_x, G_y) \approx 0$  in TrisOH, exchange interactions between other orbital states (via  $L_x$  and  $L_y$ ) would have negligible contributions in the antisymmetric exchange interaction.

S1) and the two terms in eq 19 would cancel out, leading to zero  $G_z$ . Thus, the structure of TrisOH allows there to be a nonzero  $G$  component. Similar expressions are obtained for the antisymmetric exchange between the remaining metal pairs,  $G_z^{23}$  and  $G_z^{31}$ . In TrisOH,  $G_z^{12} = G_z^{23} = G_z^{31} = G_z$  (in eq 15), and the effective sum of these two-center interaction parameters in the symmetric trigonal systems equal  $\sqrt{3}G_z$ .<sup>20,23</sup>

Finally, the amplitude of  $G_z$  is governed by the superexchange integral  $J_{x^2-y^2, x^2-y^2}^{xy, x^2-y^2}$  (or  $J_{x^2-y^2, x^2-y^2}^{x^2-y^2, xy}$ ) as described by eq 22. Thus, a large antisymmetric exchange requires the ground-to-ground state exchange ( $x^2 - y^2/x^2 - y^2$ ) and the ground-to-excited state exchange ( $x^2 - y^2/xy$ ) interactions to be both effective and comparable in magnitude (Scheme 3). To meet such criteria, the orbital superexchange pathways between each metal pair interaction must be efficient in both orbital exchange cases.

## Discussion

The present study defines the ground state of a  $\text{Cu}^{\text{II}}_3$  complex with crystallographically imposed 3-fold symmetry. With the use of VT MCD and VTVH MCD, the low-lying excited  $S = 1/2$  state split from the  ${}^2\text{E}$  ground state of the trimer has been identified and the associated zero-field splitting ( $\Delta$ ) has been accurately determined. If the effects of symmetry lowering are ignored, VT/VTVH MCD proved to be a sufficient method for determining the antisymmetric exchange parameter ( $G$ ), as  $\Delta$  is solely dependent on  $G$ . However, the combination of VT/VTVH MCD and powder/single-crystal EPR spectra has demonstrated the presence of a nonzero symmetry lowering factor ( $\delta$ ) in TrisOH and has allowed accurate determination of both the  $G$  and  $\delta$  values. Finally, the availability of accurate estimates of  $G$  and  $\delta$  has allowed a detailed description of the wave function of the trimer ground  $S = 1/2$  state and direct evaluation of the spin distribution among the three metal sites.

The microscopic determination of  $G$ ,  $\delta$ , and  $\Delta$  for this trinuclear metal cluster is possible through the unprecedented observations of the markedly low effective  $g$ -values (down to  $\sim 1.2$ ) in the single-crystal EPR spectra and the unique nesting behavior of the  $S_{\text{tot}} = 1/2$  VTVH MCD saturation curves at temperatures above 30 K. Previous studies of  $G$  relied on macroscopic magnetic susceptibility measurements<sup>6,7,22</sup> or powder pattern EPR spectra<sup>7,23</sup> which are insufficient in determining reliable values of these parameters. Moreover, these studies either ignored the effect of the symmetry lowering or dealt with very nonsymmetric systems which obfuscated the determination of the  $G$  values. Furthermore, this is the first time that the low-lying  $S = 1/2$  excited state has been directly observed and the zero-field splitting of the  ${}^2\text{E}$  state measured.

The large magnitude of  $G$  in TrisOH originates from the presence of efficient orbital superexchange pathways, both in the ground-to-ground state and in the ground-to-excited-state exchange mechanisms, via strong  $\sigma$ -type bonds with the bridging oxygen p-orbitals. Using eq 22, with the experimental  $G_z$  ( $= G$ ) of  $\sim 36 \text{ cm}^{-1}$  and  $\Delta g_z$  ( $= 2\lambda\langle x^2 - y^2 | L_z | xy \rangle^2 / E_{x^2-y^2}^{xy}$ ) of 0.32 (from EPR), one can estimate the value of  $|J_{x^2-y^2, x^2-y^2}^{xy, x^2-y^2}|$  to be  $\sim 60 \text{ cm}^{-1}$ , which is similar to the ground state isotropic exchange parameter  $|J|$  of  $\sim 105 \text{ cm}^{-1}$ . This indicates that the  $x^2 - y^2/xy$  orbital pathway is comparable to the  $x^2 - y^2/x^2 - y^2$  orbital pathway in TrisOH.

Figure 7 shows the unoccupied spin-up molecular orbital of the broken-symmetry wave functions of TrisOH best described

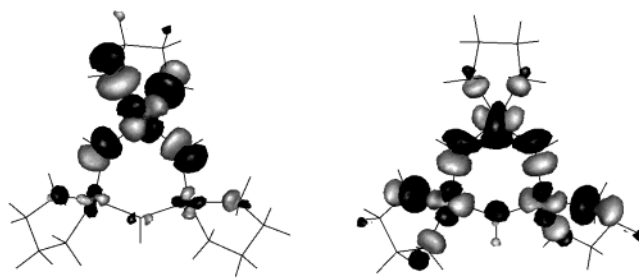


**Figure 7.** Boundary surface plots of the broken-symmetry wave functions of TrisOH for unoccupied spin-up MO localized at the  $x^2 - y^2$  orbital of the top Cu site (left) and occupied spin-up MO delocalized over all three Cu sites with the  $xy$  orbital at the top Cu site and the  $x^2 - y^2$  orbitals at the bottom two Cu sites (right). Both the  $x^2 - y^2$  and  $xy$  orbitals of the top Cu have efficient superexchange pathways with the  $x^2 - y^2$  orbitals of the other two Cu sites through  $\sigma$ -type bonds of the in-plane p-orbitals of the bridging hydroxides.<sup>50</sup>

by three  $x^2 - y^2$  orbitals with the spin density mostly localized at the top Cu site (left) and the occupied spin-up molecular orbital in which the spin density is evenly distributed over the three Cu sites with the  $xy$  orbital at the top Cu and the  $x^2 - y^2$  orbitals at the bottom two Cu's (right). The former illustrates the orbital superexchange pathways involved in the ground-to-ground state exchange, and the latter, in the ground-to-excited state exchange.<sup>50</sup> The in-plane oxygen p-orbitals along the metal–metal bonds form strong  $\sigma$ -type bonds with both the  $x^2 - y^2$  and  $xy$  orbitals. This derives from the Cu–O–Cu angle of  $144.2^\circ$  and the  $120^\circ$  rotation of  $x^2 - y^2_2$  with respect to  $x^2 - y^2_1$ . Thus, it is apparent that the antiferromagnetic exchange interactions of the two ground  $x^2 - y^2$  orbital states and that of one ground  $x^2 - y^2$  and one excited  $xy$  orbital state are similarly effective in the TrisOH structure, and as a result, a large antisymmetric exchange is obtained, but lower than in the ground state due to the first-order perturbation coefficient in eq 22.

Comparison with a recent report on a  $\text{Cu}^{\text{II}}_3$  complex by Cage et al.<sup>10</sup> exemplifies the importance of the superexchange between the ground  $x^2 - y^2$  and the excited  $xy$  orbitals. In this structure, the  $xy$  plane of each metal site is perpendicular to the  $\text{Cu}_3$  plane. Such a structure leads to orthogonal  $x^2 - y^2/xy$  orbital pairs resulting in an ineffective ground-to-excited state superexchange interactions, and thus, weak antisymmetric exchange. Analysis of the EPR data on this complex only required symmetry lowering, implying that the antisymmetry exchange is small. Alternatively, the  $x^2 - y^2/x^2 - y^2$  orbital pairs form good ground state superexchange pathways through  $\sigma$ -type bonds facilitated by two bridging carboxylate ligands between each metal pair, and thus, a strongly antiferromagnetically coupled ground state with  $J \approx -107 \text{ cm}^{-1}$  results. This illustrates that the customary estimation of the  $G$  value<sup>26</sup> as  $\propto (\Delta g/g)|2J|$  can be misleading, as the  $J$  in this formulation is just the ground state isotropic exchange parameter. Similar arguments can be formulated for the anisotropic (or pseudo-dipolar coupling) exchange interactions in dimeric copper complexes.<sup>12,51,52</sup> For example, the experimental determination of excited state exchange coupling

(50) Details of the broken-symmetry wave functions from DFT electronic calculations will be presented in ref 37.

(51) Ross, P. K.; Allendorf, M. D.; Solomon, E. I. *J. Am. Chem. Soc.* **1989**, *11*, 4009–4021.

(52) (a) Banci, L.; Bencini, A.; Gatteschi, D. *J. Am. Chem. Soc.* **1983**, *105*, 761–764. (b) Banci, L.; Bencini, A.; Gatteschi, D. *Inorg. Chem.* **1984**, *23*, 2138–2141. (c) Charlot, M.-F.; Journaux, Y.; Kahn, O.; Bencini, A.; Gatteschi, D.; Zanchini, C. *Inorg. Chem.* **1986**, *25*, 1060–1063.

parameters in dimeric copper acetate pyrazine has clearly demonstrated that the different exchange pathways would have distinctly different contributions to the total anisotropic exchange and, thus, to the zero-field splitting of the triplet ground state of the dimer.<sup>51</sup>

Rather unexpected was the presence of symmetry lowering, as the structure of the TrisOH molecule was determined to have rigorous  $D_3$  symmetry. Symmetry lowering is required to explain the experimental data, in particular, the interpretation of the EPR spectra. In fact, such behavior in homonuclear trimeric metal complexes has been previously observed.<sup>24</sup> The possibility of magnetic Jahn–Teller effect has been proposed, suggesting that a distortion of  $\sim 0.01$  Å should occur in the ground state of any antiferromagnetically coupled trinuclear complexes to remove the 3-fold symmetry.<sup>31</sup> Cage et al.<sup>10</sup> have attributed the symmetry lowering they observed to such a Jahn–Teller effect. For the TrisOH system, the effective  $D_3$  symmetry reflects either a dynamic or a static Jahn–Teller distortion where the latter would be distributed over the three orientations. However, the low Jahn–Teller stabilization energy ( $\sim 4$ – $5$  cm<sup>-1</sup>) and small structural distortion ( $\sim 0.01$  Å) make it difficult to distinguish these effects even through very low-temperature crystallography.

In TrisOH, the symmetry lowering effect is found to only partly localize the spin density on one of the metal sites in the ground  $S = 1/2$  state. This effect competes with the antisymmetric exchange, which acts to delocalize the spin density equally over the three metals. Thus, the present study finds two mechanisms for the elimination of the spin-frustration in the ground state of a trigonal metal cluster, antisymmetric exchange

with spin delocalization and the magnetic Jahn–Teller distortion with spin localization.

This investigation has been carried out as a part of an effort to elucidate the reaction mechanism of the multicopper oxidases. In particular, TrisOH is the best model for one of the two possible structures<sup>14,15e</sup> of the native intermediate form of these enzymes trapped upon dioxygen reduction. The fundamental description of the ground state of a strongly antiferromagnetically coupled Cu<sup>II</sup><sub>3</sub> cluster and insight into the superexchange pathways between different metal d-orbitals will allow a better understanding of the nature of this intermediate. This is important with respect to both the molecular mechanism of O–O bond cleavage and the contribution of the superexchange pathways to the facile reduction of this fully oxidized “native intermediate” in the turnover of the multicopper oxidases.

**Acknowledgment.** This paper is dedicated to Professor Philipp Gülich on the occasion of his 70th birthday. This research was supported by NIH Grants DK31450 (E.I.S.) and GM50730 (T.D.P.S.). L.M.M. gratefully acknowledges a John Stauffer Stanford Graduate Fellowship.

**Supporting Information Available:** Temperature dependence of powder X-band EPR spectra (3.66–100 K), powder Q-band EPR spectrum at 10 K, the comparison between 1.78 K VTVH MCD saturation curve and an  $S = 1/2$  Brillouin curve, the hyperfine pattern simulation of powder EPR, and the spin–orbit coupling scheme for a metal dimer with a center of inversion. This material is available free of charge via the Internet at <http://pubs.acs.org>.

JA046380W